Proceedings of the ASME 2024
International Design Engineering Technical Conferences and
Computers and Information in Engineering Conference
IDETC-CIE2024
August 25-28, 2024, Washington, DC

DETC2024-143807

PRESSURE-CORRECTION BASED TRANSIENT MODELING OF WAVE ENERGY POWERED REVERSE OSMOSIS (RO) DESALINATION

Xian Wu, Xiaofan Li, Lei Zuo*

[1] *Department of Naval Architecture & Marine Engineering, University of Michigan, Ann Arbor, MI 48109, USA* (leizuo@umich.edu)

ABSTRACT

Ocean wave-powered reverse osmosis (RO) desalination is an emerging field of study that combines the utilization of ocean energy and RO desalination techniques. However, due to the significant fluctuations in pressure and flow rate within the hydraulic system, an accurate transient model is necessary to estimate its performance accurately and effectively. This paper presents a two-dimensional transient model based on the pressure-correction algorithm to simulate the channel flow with porous walls and time-dependent inlet conditions. The coupled pressure, velocity, and salt concentration problem is solved iteratively by decoupling each term and updating them separately. The model is validated by comparing the results with analytical film theory which estimates the formation of the concentration polarization layer under constant inlet conditions. The performance of the RO systems, especially the concentration polarization phenomenon at the member surface, is investigated using different input conditions, including constant flow condition and sinusoidal flow condition. The salt concentration and permeate flux at the membrane boundary are studied to understand the effect of the dynamic inputs. Results show that the system can reach a higher maximum wall concentration and higher average recovery ratio in sinusoidal signal compared with the constant input. The model's adaptability to different flow regimes, from steady to sinusoidal, underscores its potential as a valuable tool in optimizing RO desalination powered by ocean wave energy.

Keywords: Transient model, reverse osmosis desalination, pressure correction, concentration polarization

1. Introduction

Reverse osmosis (RO) desalination has been widely used with more than 60% worldwide installed capacity among all the seawater processes [1], which relies on the high input pressure to drive the water against the osmotic pressure gradient across the semi-permeable membrane [2]. However, RO plants consume significant energy, ranging from 2 to 6 kWh per cubic meter for seawater desalination [3], prompting numerous studies to optimize energy usage [4]. Renewable energy sources have been identified as a promising avenue to power desalination plants without the accompanying high carbon footprint [5]. Ocean wave energy, with its impressive energy density [6] and the advantageous proximity to seawater, is increasingly recognized as a promising power source to drive RO systems sustainably.

Numerous studies have explored the potential of harnessing wave energy to power desalination systems, offering a sustainable solution for freshwater production. Researchers have developed numerical models [7-8] and built physical models [9-10] to analyze the feasibility and design of wave energy-driven RO desalination plants. Location-specific assessments have been conducted, evaluating the socioeconomic and environmental benefits in areas like Sicily [11] and Madagascar [12]. System configurations have been proposed, such as the overtopping breakwater for wave energy conversion [12] and high-efficiency batch RO [13]. Comparative studies have analyzed the performance of wave energy versus wind energy powered desalination systems [14].

While wave-powered desalination systems experience large pressure fluctuations, most previous models have assumed steady-state conditions or used constant parameters. Cheddie et al. [15] highlighted the importance of understanding the dynamic behavior of RO systems in response to varying energy inputs through transient modeling. However, their oversimplified one-dimensional model could not accurately predict the concentration polarization phenomenon [16], where salt ions accumulate near the membrane surface.

To address this limitation, researchers have developed more advanced numerical models to characterize the transient behavior and concentration polarization effects in RO desalination modules. Anqi et al. [17] numerically characterized flux performance, concentration polarization, and potential fouling sites in hollow fiber RO membranes. Su et al. [18] studied concentration polarization and permeate flux variation in a vibration-enhanced RO module. Joseph et al. [19] conducted dynamic simulations of the RO process for seawater using

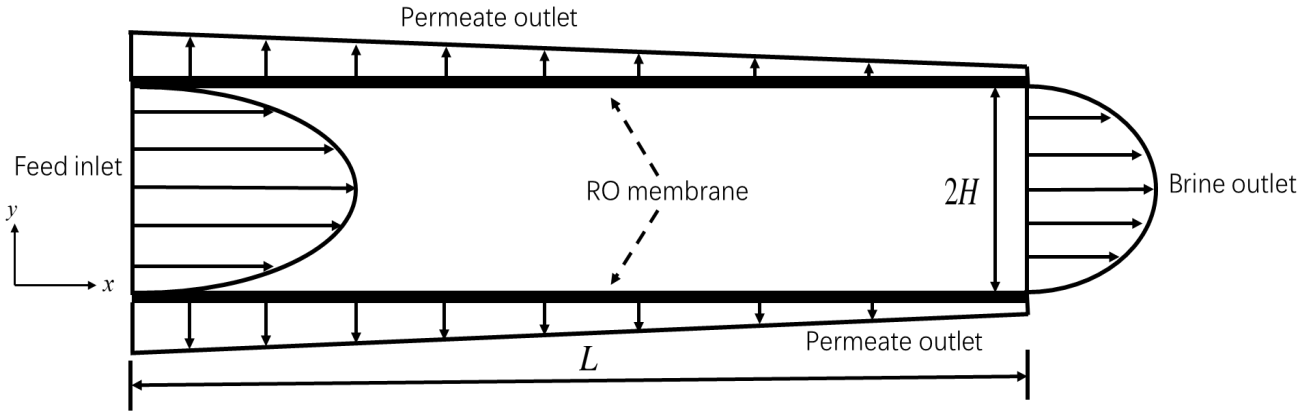

Figure 1: Flow in channel with two porous walls (RO membrane)

LabVIEW. These efforts aim to improve the understanding and modeling of transient phenomena in desalination systems. More specifically, some numerical approaches have been down trying to predict the dynamic of concentration polarization. Kim et al. developed numerical model which enables local description of permeate flux and solute rejection in crossflow reverse osmosis separations [20]. Yu et.al uses two-dimensional CFD model to predict concentration polarization under different hydraulic conditions [21]. Madireddi et al. developed an unsteady-state model to predict concentrations polarization in commercial spiral wound membranes [22] assuming a constant pressure drop.

Despite the advancements in computational modeling of RO desalination, a gap remains in fully understanding how these systems respond to dynamic conditions, particularly those influenced by wave-generated energy with its characteristic sinusoidal inputs. While certain research, like the work by Alexiadis et al. [23], has ventured into dynamic modeling of high-pressure RO under pulse disturbances, and Cheddie et al. [15] have explored the concentration polarization effects using a simplified one-dimensional approach, comprehensive studies incorporating the multifaceted and fluctuating inputs typical of wave energy are lacking. Recognizing this deficiency, it becomes clear that there is a compelling need for more sophisticated and accurate transient RO models that can represent the system behaviors under the variable flow conditions.

In this paper, a transient two-dimensional model is developed to simulate the channel with two porous walls under time-varying pressure and flow conditions. The model is based on iterative pressure correction scheme considering the salt diffusion in the channel and boundary at RO membrane surface coupling pressure, velocity, and salt concentration fields. The model is validated with the analytical solution from film theory. Two different flow conditions, including constant and sinusoidal inlet conditions are investigated with the formation of the concentration polarization layer.

The paper is organized as follows: The transient two-dimensional model is presented in Section 2 with the numerical approach introduced in Section 3. Two different input signals with varying pressure and flow rate are investigated and compared in Section 4 with the model validation. The method and results are concluded finally in Section 5.

2. Model Description

A 2D rectangle channel (as shown in Figure. 1) is used to develop the model in this study, with the two porous walls on each side of the channel. Here the porous walls can be considered as two flat sheet membranes (or unwound spiral wound membrane).

2.1 Governing Equations

Ignoring the density change (less than 1% change), body force (such as gravity), and turbulence effect (low Reynolds number) in the process, assuming incompressible flow, the expanded continuity, and Navier-Stokes equations (in x and y directions) are as follows:

$$\frac{\partial u}{\partial x}+\frac{\partial v}{\partial y}=0 \tag{1}$$

$$\frac{\partial u}{\partial t}+\frac{\partial u^2}{\partial x}+\frac{\partial uv}{\partial y}=-\frac{\partial p}{\rho\partial x}+\nu\left(\frac{\partial^2 u}{\partial x^2}+\frac{\partial^2 u}{\partial y^2}\right) \tag{2}$$

$$\frac{\partial v}{\partial t}+\frac{\partial uv}{\partial x}+\frac{\partial v^2}{\partial y}=-\frac{\partial p}{\rho\partial y}+\nu\left(\frac{\partial^2 v}{\partial x^2}+\frac{\partial^2 v}{\partial y^2}\right) \tag{3}$$

where u and v are the velocities parallel to and vertical with the channel direction, t is time, p is the pressure, ρ is the liquid density, and ν is the kinematic viscosity. The diffusion equation of the salt concentration can be written as follows:

$$\frac{\partial c}{\partial t}+\frac{\partial(uc)}{\partial x}+\frac{\partial(vc)}{\partial y}=D\left(\frac{\partial^2 c}{\partial x^2}+\frac{\partial^2 c}{\partial y^2}\right) \tag{4}$$

where c is the salt concentration in the solution, and D is the solution diffusivity.

2.2 Boundary Conditions

Because the feed inlet boundary is time dependent and the membranes are semipermeable, the Boundary Conditions (B.C.s) in the presented channel flow problem are rather complex. Three types of B.C.s are used in the simulation: inlet boundary, outlet boundary, and membrane boundary.

2.2.1 Inlet Boundary (at x=0)

The following B.C.s are used to set the time dependent inlet boundary (left boundary of the channel):

$$p_{x=0} = p(t) \tag{5}$$

$$c_{x=0} = c_0 \tag{6}$$

where $p(t)$ is time dependent pressure function, and c_0 is the initial salt concentration. During real application, the inlet flow will always be fully developed before entering the RO membrane channel. Thus, the velocities in channels with two porous walls are used to estimate the inlet fully developed flow at inlet [24]:

$$u_{x=0} = \frac{3}{2}u(t)\left(1-\left(\frac{y-H}{H}\right)^2\right) \tag{7}$$

$$v_{x=0} = v_w \frac{y}{2H}\left(3-\left(\frac{y-H}{H}\right)^2\right) \tag{8}$$

where $u(t)$ is time dependent velocity function, H is half of the channel height, and v_w is the vertical velocity at porous wall (membrane surface) which will be defined in 2.2.3.

2.2.2 Outlet Boundary (at x=L)

The following B.C.s are used to set the outlet (right boundary of the channel):

$$\left.\frac{\partial u}{\partial x}\right|_{x=L} = 0 \text{ and } \left.\frac{\partial v}{\partial x}\right|_{x=L} = 0 \tag{9\&10}$$

$$\left.\frac{\partial p}{\partial x}\right|_{x=L} = 0 \tag{11}$$

2.2.3 Membrane Boundary (at y=0 & 2H)

The vertical velocity v_w at membrane surface (which is the water flux across membrane) can be defined as a function of local pressure and concentration:

$$v_w = \left.\frac{\partial v}{\partial x}\right|_{y=0\ \&\ 2H} = K_A\left(p_w - K_{os}\left(c_w - c_p\right)\right) \tag{12}$$

where K_A is the membrane permeability coefficient, p_w is the pressure at the membrane surface (ignoring the outside pressure change), K_{OS} is the osmosis pressure coefficient, c_w is the salt concentration at membrane surface, and c_p is the salt concentration in permeate which can be expressed as:

$$c_p = \frac{v_s}{v_w} \tag{13}$$

where v_s is the salt flux across the membrane, it can be further expressed as:

$$v_s = K_s\left(c_w - c_p\right) \tag{14}$$

where K_s is the salt flux coefficient of the membrane. As for the horizontal velocity, partial slip condition is applied in the porous surface [25]:

$$u_{y=0} = K_{slip}\left.\frac{\partial u}{\partial y}\right|_{y=0} \text{ and } u_{y=2H} = K_{slip}\left.\frac{\partial u}{\partial y}\right|_{y=2H} \tag{15}$$

where K_{slip} is the partial slip coefficient (or virtual partial slip length).

3. Numerical Approach

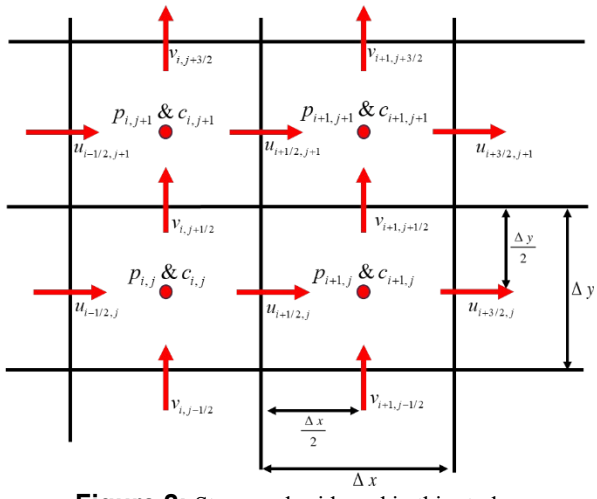

Figure 2: Staggered grid used in this study.

A staggered grid is used as shown in Figure. 2, where the scalar variables (p and c) are stored in the cell center and the velocities are located at the cell faces.

3.1 Discretized Governing Equations

A finite difference (FD) formulation is used to discretize the presented model. The time terms are discretized using first order forward differencing, while space terms are discretized using second order central differencing.

For momentum equation in x direction (Eq. 2), it can be discretized as (center from point $\left(i+\frac{1}{2},j\right)$):

$$u^{n+1}_{i+1/2,j}=u^{n}_{i+1/2,j}+A\Delta t-\frac{\Delta t}{\rho\Delta x}\left(p^{n}_{i+1,j}-p^{n}_{i,j}\right) \tag{16}$$

and

$$A=-\left[\frac{(u^2)^{n}_{i+3/2,j}-(u^2)^{n}_{i-1/2,j}}{2\Delta x}-\frac{(uv)^{n}_{i+1/2,j+1}-(uv)^{n}_{i+1/2,j-1}}{2\Delta y}\right]+\nu\left[\frac{u^{n}_{i+3/2,j}-2u^{n}_{i+1/2,j}+u^{n}_{i-1/2,j}}{\Delta x^2}+\frac{u^{n}_{i+1/2,j+1}-2u^{n}_{i+1/2,j}+u^{n}_{i+1/2,j-1}}{\Delta y^2}\right] \tag{17}$$

where Δx is the mesh size in x direction, Δt is the time step size, and the subscripts i, j and n refer to axial, transverse and time coordinates. For the velocity at center, it can be calculated as an average from nearby points, such as:

$$v_{i+1/2,j+1}=\frac{v_{i,j+1/2}+v_{i,j+3/2}+v_{i+1,j+1/2}+v_{i+1,j+3/2}}{4} \tag{18}$$

Similarly, the y-direction momentum equation can be discretized as (center from point $\left(i,j+\frac{1}{2}\right)$):

$$v^{n+1}_{i,j+1/2}=v^{n}_{i,j+1/2}+B\Delta t-\frac{\Delta t}{\rho\Delta y}\left(p^{n}_{i,j+1}-p^{n}_{i,j}\right) \tag{19}$$

and

$$B=-\left[\frac{(uv)^{n}_{i+1,j+1/2}-(uv)^{n}_{i-1,j+1/2}}{2\Delta x}+\frac{(v^2)^{n}_{i,j+3/2}-(v^2)^{n}_{i,j-1/2}}{2\Delta y}\right]+\nu\left[\frac{v^{n}_{i+1,j+1/2}-2v^{n}_{i,j+1/2}+v^{n}_{i-1,j+1/2}}{\Delta x^2}+\frac{v^{n}_{i,j+3/2}-2v^{n}_{i,j+1/2}+v^{n}_{i,j-1/2}}{\Delta y^2}\right] \tag{20}$$

where Δy is the mesh size in y direction. Substitute Eq. 16 & 18 back into continuity equation (Eq. 1), the pressure passion equation can be expressed as:

$$p_{i,j}=\frac{1}{a}\left(\frac{p_{i+1,j}}{(\Delta x)^2}+\frac{p_{i-1,j}}{(\Delta x)^2}+\frac{p_{i,j+1}}{(\Delta y)^2}+\frac{p_{i,j-1}}{(\Delta y)^2}-b\right) \tag{21}$$

where

$$a=2\left[\frac{\Delta t}{(\Delta x)^2}+\frac{\Delta t}{(\Delta y)^2}\right] \tag{22}$$

and

$$b=\frac{\rho}{\Delta t}\left(\frac{u_{i+1/2,j}-u_{i-1/2,j}}{\Delta x}+\frac{v_{i,j+1/2}-v_{i,j-1/2}}{\Delta y}\right) \tag{23}$$

Finally, the salt diffusion can be discretized centered from point (i,j):

$$c^{n+1}_{i,j}=c^{n}_{i,j}\left[1-\Delta t\left(\frac{u^{n}_{i,j}}{\Delta x}+\frac{v^{n}_{i,j}}{\Delta y}\right)-2D\Delta t\left(\frac{1}{\Delta x}+\frac{1}{\Delta y}\right)\right]+D\Delta t\left[\frac{c^{n}_{i+1,j}+c^{n}_{i-1,j}}{(\Delta x)^2}+\frac{c^{n}_{i,j+1}+c^{n}_{i,j-1}}{(\Delta y)^2}\right] \tag{24}$$

3.2 Iterative Pressure-Correction Scheme

The discretized system is explicit in time and conditionally stable. Thus, an iterative pressure correction method (as shown in Figure.3) is used to control the error while advancing in time steps. The velocity, pressure and concentration components are decoupled to update separately, where they are considered to each consist of a prediction part (-p) and a correction part (-c):

$$u=up+uc \tag{25}$$

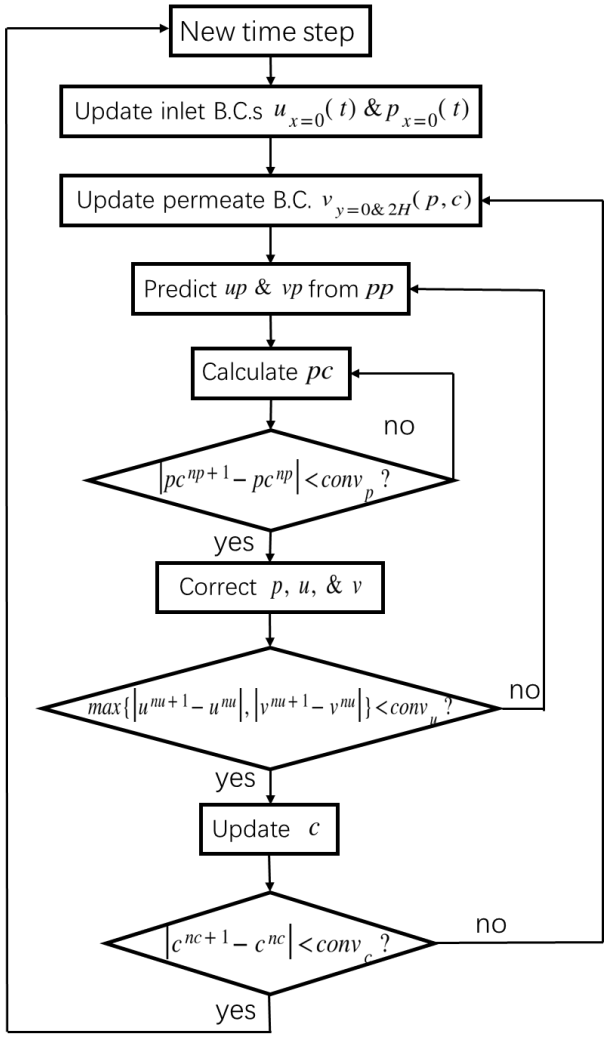

Figure 3: Flowchart of the pressure correction based iterative scheme for transient RO modeling.

$$v = vp + vc \tag{26}$$

$$p = pp + pc \tag{27}$$

$$c = cp + cc \tag{28}$$

Then the iterative scheme will converge at each time step when:

$$max(\, uc, vc, pc, cc) \rightarrow 0 \tag{29}$$

For each new time step, the pressure and concentration from previous time step will be the initial prediction value to initialize the iteration. For the first time step, a uniform concentration field and a linear drop pressure field are used as initial predictions. Meanwhile, the inlet boundary will update with the time dependent function (Eqs. 5 & 7). With each time step, 3 layers of iteration loops are used to update and correct the velocity, pressure, and concentration separately.

The concentration iteration loop will start with updating the membrane boundary condition (Eq. 12) using the prediction concentration. Secondly, the velocity iteration loop will start with predicting the velocity field based on the updated boundary conditions and predicted pressure (Eqs. 16 & 19). Finally, the pressure iteration loop will update the correction part of pressure based on the continuity (Eq. 21) till it fills the convergence criteria:

$$\left| pc^{\,np+1} - pc^{\,np} \right| < conv_{\,p} \tag{30}$$

where np is the iteration count of pressure, and $conv_{\,p}$ is the convergence limit for pressure.

After the correction of pressure converges to a certain value, the pressure can be updated based on Eq. 27:

$$p = pp + K_{\,p} \cdot pc \tag{31}$$

where $K_{\,p}$ is the pressure relaxation factor (taken from 0 to 1). From Eq. 16 & 19, the correction part of velocity can be calculated from correction of pressure:

$$uc_{\,i+1/2,j} = -\frac{\Delta t}{\rho \Delta x}\left(pc_{\,i+1,j} - pc_{\,i,j} \right) \tag{32}$$

and

$$vc_{\,i,j+1/2} = -\frac{\Delta t}{\rho \Delta y}\left(pc_{\,i,j+1} - pc_{\,i,j} \right) \tag{33}$$

Then, the velocity can be updated based on Eq. 25 & 26:

$$u = up + K_{\,u} \cdot uc \tag{34}$$

$$v = vp + K_{\,u} \cdot vc \tag{35}$$

where $K_{\,u}$ is the velocity relaxation factor. The velocity convergence limit $conv_{\,u}$ is the iteration check for the velocity inner loop:

$$max\{ \left| u^{\,nu+1} - u^{\,nu} \right|, \left| v^{\,nu+1} - v^{\,nu} \right| \} < conv_{\,u} \tag{36}$$

where nu is the iteration count for velocity.

After update and converge pressure and velocity, the concentration can be updated based on Eq. 24, with the convergence check as:

$$\left| c^{\,nc+1} - c \right| < conv_{\,c} \tag{37}$$

where nc is the iteration count for concentration, and $conv_{\,c}$ is the concentration convergence limit. If the updated concentration passes the convergence check, all fields have been updated and converged, which can mover to next time step.

Following the proposed pressure based iterative scheme, the coupled concentration, velocity, and pressure field can be updated sequentially with separate convergence check to ensure the stability of the entire calculation.

4. Results and Discussion

Table 1: Constant parameters used in this paper.

Constant	Value	Units
$c_{\,0}$	2	$kg\ m^{-3}$
ρ	1035	$kg\ m^{-3}$
D	7.5×10^{-9}	$m^2 s^{-1}$
ν	9.372×10^{-7}	$m^2 s^{-1}$
L	0.2	m
H	0.001	m
$K_{\,u}$	0.6	–
$K_{\,p}$	0.2	–
$conc_{\,p}$	10^{-6}	Pa
$conc_{\,u}$	10^{-7}	$m\ s^{-1}$
$conc_{\,c}$	10^{-5}	$kg\ m^{-3}$
$K_{\,a}$	9.72×10^{-12}	$m\ Pa^{-1}\ s^{-1}$
K_{OS}	77930	$J\ kg^{-1}$
$K_{\,s}$	3.5×10^{-7}	$m\ s^{-1}$
K_{slip}	2×10^{-8}	m

The presented iterative pressure correction scheme solving the coupled 2D channel desalination model is calculated in a finite difference script using MATLAB. The following constant parameters are used during the simulation as shown in Table. 1.

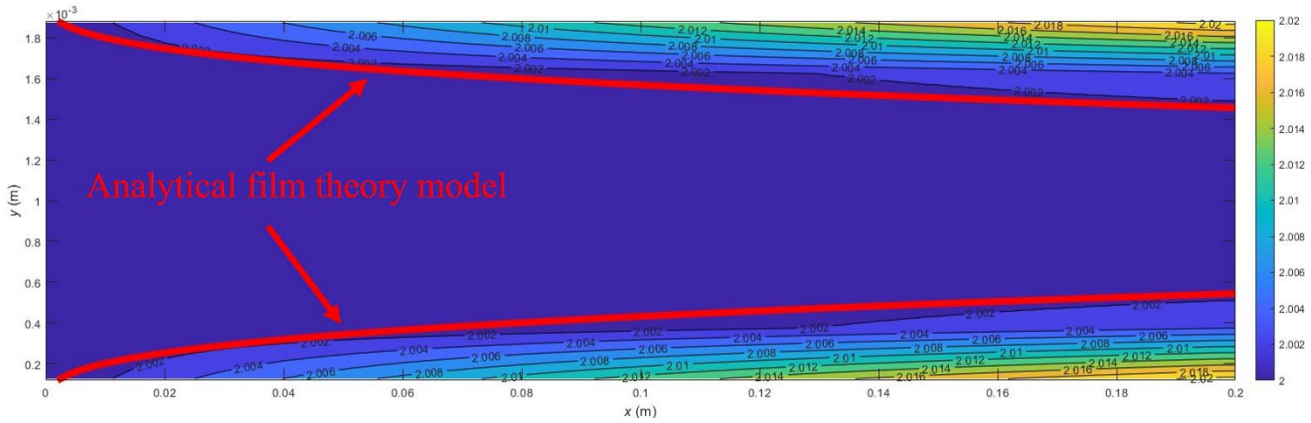

Figure 4: Salt concentration contour under constant inlet condition. The red line is the analytical solution for concentration polarization layer thickness from film theory.

4.1 Model Validation under Constant Input

The presented model is validated using the film theory developed by Michaels and others [26]. Film theory simplifies the complex coupled problem by neglecting axial solute convection near the membrane surface. The thickness of the concentration polarization layer thus can be solved analytically, especially in a channel with soluble walls [27]. For the fully developed laminar flow in a thin rectangular channel, the film thickness can be expressed as:

$$\delta(x) = 1.475x\left(\frac{H}{x}\right)^{2/3}\left(\frac{D}{u_{max}H}\right)^{1/3} \qquad (38)$$

where $\delta(x)$ is the thickness of the concentration polarization layer, and u_{max} is the maximum horizontal velocity in the channel.

To be comparative with the results from the film theory, the system is firstly simulated under constant input conditions:

$$\begin{cases} P_{x=0} = P_0 \\ u_{x=0} = U_0 \cdot \frac{3}{2}\left(1-\left(\frac{y-H}{H}\right)^2\right) \end{cases} \qquad (39 \& 40)$$

where $P_0 = 9\times 10^5\, Pa$, and $U_0 = 3\times 10^{-2} m\cdot s^{-1}$.

Mesh size convergence check has been done, where $\Delta x = 2\times 10^{-3}\, m$, $\Delta y = 2.5\times 10^{-4} m$, and $\Delta t = 1.5\times 10^{-5} s$ are chosen in this case. By checking the contour of concentration after the concentration polarization layer is fully developed, the concentration polarization layer thickness from the simulation fits well with the calculated from the film theory (Figure. 4). The little difference is mainly caused by the ignored convection in the analytical solution.

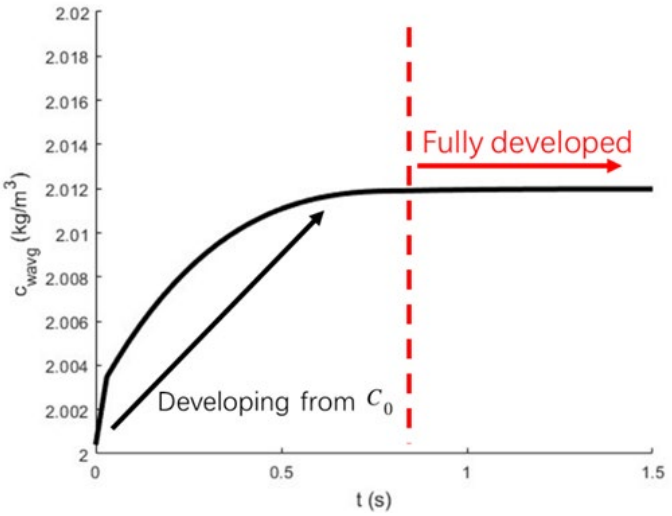

Figure 5: Development of average wall concentration over time under constant inlet condition

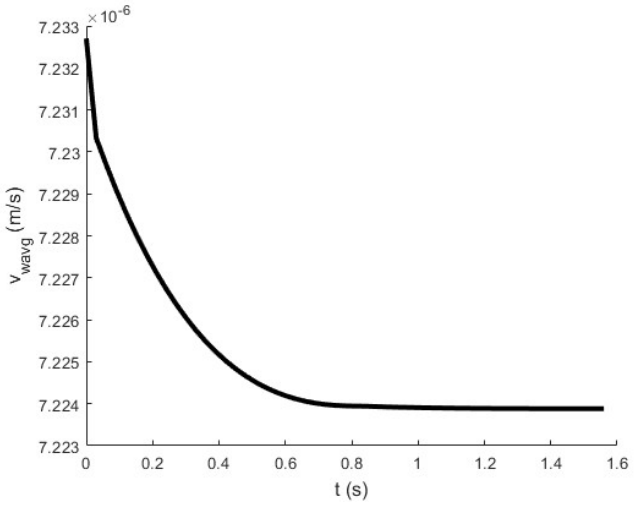

Figure 6: Average velocity at porous wall surface over time

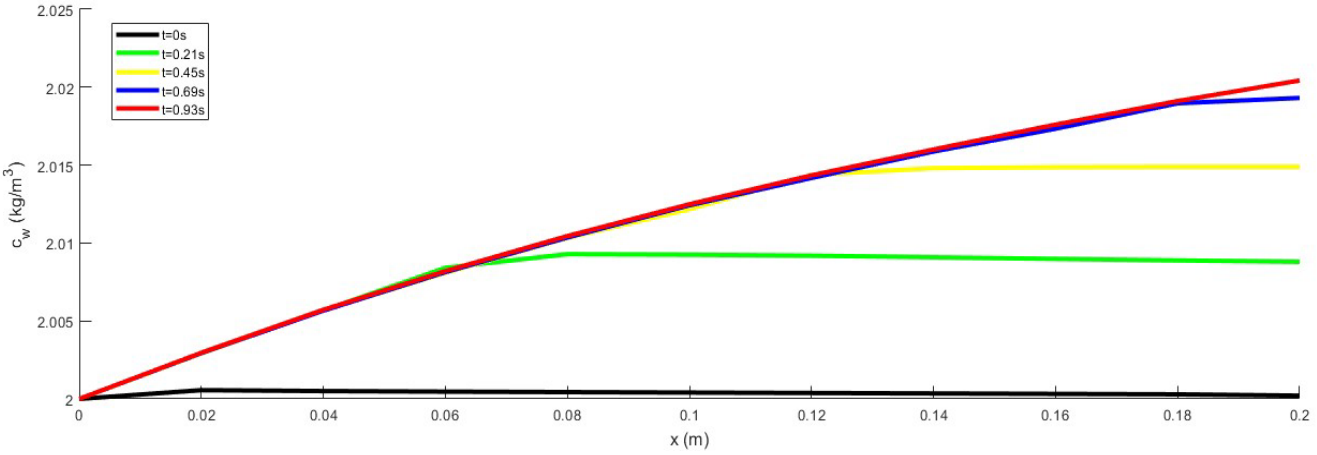

Figure 7: Wall concentration along the channel at different time under constant inlet condition

The average wall concentration c_{wavg} increases fast from c_0 to a stable value (around 1 s), where the diffusion mainly from wall to channel center is in balance with the flow convection mainly from channel center to the wall (Figure.5). Because of the fast increase in c_{wavg}, the permeate flux (in terms of average wall velocity v_{wavg}) will reduce to overcome more osmotic pressure from the high density (as shown in Figure. 6).

The development of the wall concentration is better described in Figure. 7, where the wall concentration along x direction is plotted in 5 different times. From 0s, c_w increases from c_0, and will be developed first at the inlet side of the channel. As for the outlet side of the channel, c_w will continuously increase but not across the wall concentration in nearest upstream which does not reach its maximum yet. It is because when the salt concentration in any upstream point does not reach its maximum limit (balance of diffusion and convection), that downstream point will lose wall concentration through diffusion earlier than expected. But when the upstream side all reaches their maximum wall concentration, the downstream point will not lose extra wall concentration through diffusion, which accelerates its growth to its own maximum wall concentration.

4.2 Response under Sinusoidal Input

Considering a dual acting piston pump is used to pressurize the inlet flow (can be driven either the wave energy converter or human), a coupled simplified sinusoidal input condition is used:

$$\begin{cases} P_{x=0} = P_1 + P_2 \cdot \left|\sin(wt)\right| \\ u_{x=0} = \left(U_1 + U_2 \cdot \left|\sin(wt)\right|\right) \dfrac{3}{2}\left(1 - \left(\dfrac{y-H}{H}\right)^2\right) \end{cases} \quad (41\&42)$$

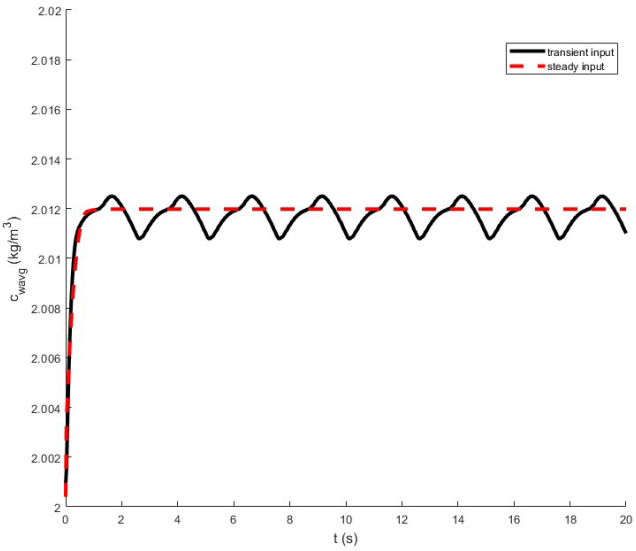

Figure 8: Average wall concentration over time under sinusoidal input condition.

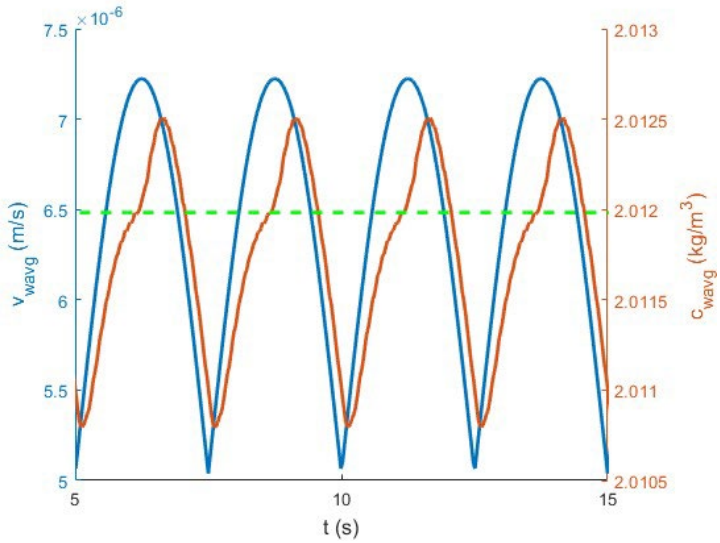

Figure 9: Average velocity at porous wall along the average wall concentration over time. The green line is the average wall concentration under steady condition.

where $P_1 = 6.75 \times 10^5\ Pa$, $P_2 = 2.25 \times 10^5\ Pa$, $U_1 = 2.25 \times 10^{-3}\ m \cdot s^{-1}$, $U_2 = 7.5 \times 10^{-4}\ m \cdot s^{-1}$, ω is the fluctuation frequency. Consider driven by an ocean energy converter in east coast of U.S., ω is taken as $\frac{2\pi}{5} s^{-1}$, assuming 5 seconds of wave near shore. Accounting the effect of pressure accumulator and avoiding considering the backwashing phenomenon at this stage, the system is set above a minimum pressure larger than the osmotic pressure.

The response of c_{wavg} over time is plotted in Figure. 8. Initially, the c_{wavg} follows a similar trend as the trend from the previous steady case study. However, after it reaches the maximum concentration limit in steady case, c_{wavg} under the sinusoidal input can still increase.

Also, it's worth noticing that when c_{wavg} can increase cross the steady state limit is always when the pressure is dropping. It is because the drop of channel pressure leads to drop of water flux across membrane. Meanwhile, more salt can stay inside the channel to increase the wall concentration. The water flux across membrane is plotted in Figure. 9 together with the average wall concentration, to better compare the time and change in each value.

4.3 Recovery Ratio

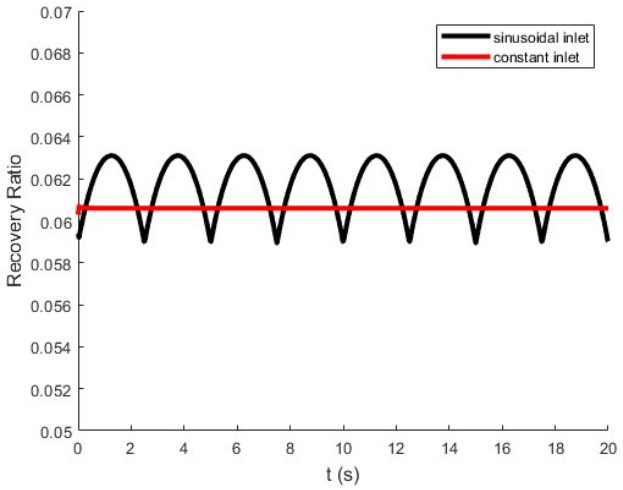

Figure 10: Recovery ration under two inlet conditions over time.

The formation of the concentration polarization in both steady and sinusoidal inputs has been investigated, along with the permeate flux changes. To better evaluate the effectiveness of the two different signals, a simplified Recovery Ratio (RR), which is the ratio of permeate flux and feed flux can be expressed as:

$$RR = \frac{\bar{v}_w L}{\bar{u}_{out} H + \bar{v}_w L} \tag{43}$$

where $\bar{u}_{out}$ is the average velocity at outlet in x direction. Before comparing the results from the two different inputs conditions, another constant input condition is used for the fair comparison, where in the constant boundary conditions (Eq.39& 40) $P_0 = 8.183 \times 10^5\ Pa$, and $U_0 = 2.72 \times 10^{-2} m \cdot s^{-1}$. So, the updated constant inlet and the sinusoidal inlet have same average pressure and velocity over time.

RRs from the two different signals are plotted in Figure. 10. The constant inlet condition has a lower recovery ratio due to a more stable concentration polarization layer, which fits the conclusion in previous study [15] that the dynamic response brings larger recovery ratio (about 2% increase in this case).

5. Conclusion

This paper developed a pressure correction based transient two-dimensional model for reverse osmosis desalination, which applies a rectangle channel with two porous walls (RO membrane). The model was based on an iterative pressure-correction method, which decouples the velocity, pressure, and salt concentration fields and updates them separately. By simulating the formation of the concentration polarization layer under constant inlet conditions, the model is validated comparing with the analytical solution from the film theory. Meanwhile, by simulating the transient flow conditions and their effects on the wall concentration and velocity, the model provides insights into optimizing system performance, emphasizing the importance of addressing concentration polarization. The model's robustness and adaptability to various operational conditions exemplify its utility in guiding the design and optimization of future desalination systems.

The current model can be further improved to include membrane surface scaling and backwashing phenomenon. More flow conditions and their response are worth investigating using the presented model.

ACKNOWLEDGEMENTS

The authors wish to thank the support from National Science Foundation (award numbers #2246608).

REFERENCES

[1] V. Pankratz, F. Gasson TJ., IDA Desalination Yearbook 2015–2016, Oxford, UK, Global Water Intell, 2016.

[2] Helfer, Fernanda, Charles Lemckert, and Yuri G. Anissimov. "Osmotic power with pressure retarded osmosis: theory, performance and trends–a review." Journal of membrane science 453 (2014): 337-358.

[3] Panagopoulos, Argyris. "A comparative study on minimum and actual energy consumption for the treatment of desalination brine." Energy 212 (2020): 118733.

[4] Avlonitis, S. A., K. Kouroumbas, and N. Vlachakis. "Energy consumption and membrane replacement cost for seawater RO desalination plants." Desalination 157.1-3 (2003): 151-158.

[5] Koroneos, C., A. Dompros, and G. Roumbas. "Renewable energy driven desalination systems modelling." Journal of cleaner production 15, no. 5 (2007): 449-464.

[6] Li, Zhenyu, Afreen Siddiqi, Laura Diaz Anadon, and Venkatesh Narayanamurti. "Towards sustainability in water-energy nexus: Ocean energy for seawater desalination." Renewable and Sustainable Energy Reviews 82 (2018): 3833-3847.

[7] Folley, Matt, Baltasar Peñate Suarez, and Trevor Whittaker. "An autonomous wave-powered desalination system." Desalination 220, no. 1-3 (2008): 412-421.

[8] Yu, Yi-Hsiang, and Dale Jenne. "Numerical modeling and dynamic analysis of a wave-powered reverse-osmosis system." Journal of marine science and engineering 6, no. 4 (2018): 132.

[9] Magagna, Davide, and Gerald Muller. "A wave energy driven RO stand-alone desalination system: initial design and testing." Desalination and Water Treatment 7, no. 1-3 (2009): 47-52.

[10] Mi, Jia, Xian Wu, Joseph Capper, Xiaofan Li, Ahmed Shalaby, Ruoyu Wang, Shihong Lin, Muhammad Hajj, and Lei Zuo. "Experimental investigation of a reverse osmosis desalination system directly powered by wave energy." Applied Energy 343 (2023): 121194.

[11] Viola, Alessia, Vincenzo Franzitta, Marco Trapanese, Domenico Curto, and D. Viola. "Nexus water & energy: A case study of wave energy converters (WECs) to desalination applications in Sicily." Int. J. Heat Technol 34, no. 2 (2016): S379-S386.

[12] Contestabile, Pasquale, and Diego Vicinanza. "Coastal defence integrating wave-energy-based desalination: A case study in Madagascar." Journal of Marine Science and Engineering 6, no. 2 (2018): 64.

[13] Brodersen, Katie M., Emily A. Bywater, Alec M. Lanter, Hayden H. Schennum, Kumansh N. Furia, Maulee K. Sheth, Nathaniel S. Kiefer et al. "Direct-drive ocean wave-powered batch reverse osmosis." Desalination 523 (2022): 115393.

[14] Pedro Cabrera; Matt Folley; José A. Carta; "Design and Performance Simulation Comparison of A Wave Energy-powered and Wind-powered Modular Desalination System", DESALINATION, 2021. (IF: 3)

[15] Cheddie, Denver, Aatma Maharajh, Aneil Ramkhalawan, and Prakash Persad. "Transient modeling of wave powered reverse osmosis." Desalination 260, no. 1-3 (2010): 153-160.

[16] Matthiasson, Einar, and Björn Sivik. "Concentration polarization and fouling." Desalination 35 (1980): 59-103.

[17] Anqi, Ali E., Mohammed Alrehili, Mustafa Usta, and Alparslan Oztekin. "Numerical analysis of hollow fiber membranes for desalination." Desalination 398 (2016): 39-51.

[18] Su, Xu, Wende Li, Alan Palazzolo, and Shehab Ahmed. "Concentration polarization and permeate flux variation in a vibration enhanced reverse osmosis membrane module." Desalination 433 (2018): 75-88.

[19] Joseph, Arun, and Vasanthi Damodaran. "Dynamic simulation of the reverse osmosis process for seawater using LabVIEW and an analysis of the process performance." Computers & Chemical Engineering 121 (2019): 294-305.

[20] Kim, Suhan, and Eric MV Hoek. "Modeling concentration polarization in reverse osmosis processes." Desalination 186, no. 1-3 (2005): 111-128.

[21] Yu, Zhou, Xinmin Wang, Weiying Li, and Sheng Chen. "Computational Fluid Dynamics Modeling of Hollow Membrane Filtration for Concentration Polarization." Water 13, no. 24 (2021): 3605.

[22] Madireddi, K., R. B. Babcock, B. Levine, J. H. Kim, and M. K. Stenstrom. "An unsteady-state model to predict concentration polarization in commercial spiral wound membranes." Journal of Membrane Science 157, no. 1 (1999): 13-34.

[23] Alexiadis, Alessio, J. Bao, D. F. Fletcher, D. E. Wiley, and D. J. Clements. "Dynamic response of a high-pressure reverse osmosis membrane simulation to time dependent disturbances." Desalination 191, no. 1-3 (2006): 397-403.

[24] A.S. Berman, Laminar flow in channels with porous walls, J. Appl. Phys. 24 (1953) 1232±1235.

[25] Bocquet L, Charlaix E. Nanofluidics, from bulk to interfaces. Chemical Society Reviews. 2010;39(3):1073-95.

[26] A.S. Michaels, New separation technique for the CPI, Chem. Eng. Prog., 64 (1968) 31.

[27] M.C. Porter, Concentration polarization with membrane ultrafiltration, Ind. Eng. Chem. Prod. Res. Develop., 11 (1972) 234.